AD-A129 803 ACOUSTO-OPTIC FOURIER TRANSFORM DEVICES FOR SURVEILLANCE SIGNAL PROCESSING(U) NAVAL RESEARCH LAB WASHINGTON DC J N LEE ET AL. 30 JUN 83 NRL-MR-5113 1/1

UNCLASSIFIED F/G 12/1 NL

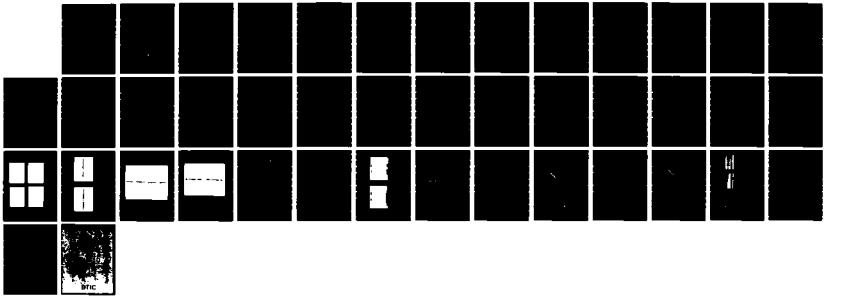

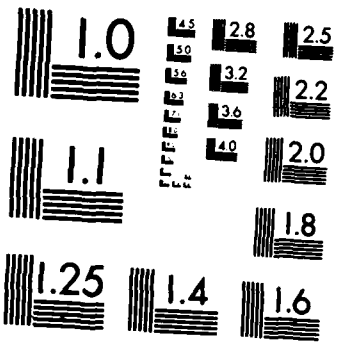

NRL Memorandum Report 5113

Acousto-Optic Fourier Transform Devices for Surveillance Signal Processing

JOHN N. LEE, S. C. LIN AND A. B. TVETEN

Applied Optics Branch
Optical Sciences Division

June 30, 1983

NAVAL RESEARCH LABORATORY
Washington, D.C.

SECURITY CLASSIFICATION OF THIS PAGE (When Data Entered)

REPORT DOCUMENTATION PAGE	READ INSTRUCTIONS BEFORE COMPLETING FORM
1. REPORT NUMBER: NRL Memorandum Report 5113 AD-A129803	2. GOVT ACCESSION NO. / 3. RECIPIENT'S CATALOG NUMBER
4. TITLE (and Subtitle): ACOUSTO-OPTIC FOURIER TRANSFORM DEVICES FOR SURVEILLANCE SIGNAL PROCESSING	5. TYPE OF REPORT & PERIOD COVERED: Interim report 10 Feb 1982 — 30 Sept 1982
	6. PERFORMING ORG. REPORT NUMBER
7. AUTHOR(s): John N. Lee, S.C. Lin and A.B. Tveten	8. CONTRACT OR GRANT NUMBER(s)
9. PERFORMING ORGANIZATION NAME AND ADDRESS: Naval Research Laboratory Washington, DC 20375	10. PROGRAM ELEMENT, PROJECT, TASK AREA & WORK UNIT NUMBERS: 62712N; WF-151-710; 65-1588-0-0
11. CONTROLLING OFFICE NAME AND ADDRESS: Naval Air Systems Command Washington, DC 20361	12. REPORT DATE: June 30, 1983
	13. NUMBER OF PAGES: 40
14. MONITORING AGENCY NAME & ADDRESS (if different from Controlling Office)	15. SECURITY CLASS. (of this report): UNCLASSIFIED
	15a. DECLASSIFICATION/DOWNGRADING SCHEDULE

16. DISTRIBUTION STATEMENT (of this Report)

Approved for public release; distribution unlimited.

17. DISTRIBUTION STATEMENT (of the abstract entered in Block 20, if different from Report)

18. SUPPLEMENTARY NOTES

19. KEY WORDS (Continue on reverse side if necessary and identify by block number)

Acousto-optics
Optical Signal Processing
Discrete and continuous Fourier transforms
Time-integrating architecture
Diode laser source
Compact construction

20. ABSTRACT (Continue on reverse side if necessary and identify by block number)

Acousto-optic techniques have been investigated for application to the Fourier-transform requirements of the Gemini surveillance concept. Acousto-optical computation of continuous and discrete Fourier transforms have been performed using a time-integrating architecture. Time-integration in conjunction with diode lasers and bulk optics can be used to produce inherently compact optical systems, and several compact

(Continues)

DD FORM 1 JAN 73 1473 EDITION OF 1 NOV 65 IS OBSOLETE
S/N 0102-014-6601

SECURITY CLASSIFICATION OF THIS PAGE (When Data Entered)

20. ABSTRACT (Continued)

processor concepts have been demonstrated. Performance parameters and tradeoffs have been analyzed for these processors, and present device limitations identified. 30 dB dynamic range has been demonstrated. Additional concepts for miniaturization, including application of integrated optics, are discussed. Multichannel operation will be required in Gemini, and the Fourier-transform devices developed here have been shown to be easily adaptable to multichannel operation. Two-channel operation has been demonstrated; several multichannel concepts have been evaluated, and one design is being implemented.

CONTENTS

ACOUSTO-OPTIC FOURIER TRANSFORM DEVICES FOR SURVEILLANCE SIGNAL PROCESSING

I. INTRODUCTION

This report covers interim progress on an effort to address the signal-processing requirements of a new surveillance technique called Gemini. This technique shows promise for high-probability optical detection of moving targets in extreme clutter environments, and initial demonstrations have been performed by Aerojet Electrosystems and Synoptics Associates. The Gemini concept, illustrated in Fig. 1, uses a two-mirror interferometer scheme whereby an imaged scene contains a fringe pattern determined by the mirror separation. An array of detectors views the imaged scene through a fixed reticle with a bar pattern of spatial periodicity equal to that of the fringes. Temporal, AC outputs are obtained from the individual detectors behind the reticle if there is movement in the field, since in that case the interferometer fringes move across the bar pattern. (An AC off-set is possible with detector system scan motion.) Targets and clutter can theoretically be distinguished by analysis of the frequency spectrum of these temporal signals. The basis for discrimination is that the background and target will result in different temporal frequencies as illustrated in Fig. 2. The Optical Transfer Function of the interferometer is multiplied by the angular velocity of the object to produce the temporal (electrical) spectrum. Since the angular velocities for background and target as shown in Fig. 2 are different, different temporal frequencies result. Target recognition is accomplished by looking for specific target frequencies. The target frequencies are typically in the 100-1000 Hz range. In practice, it is possible for the object and background spectra to overlap due to a distribution of velocities. Target recognition can then be obtained using

Manuscript approved April 25, 1983.

techniques similar to those employed on direct imagery, such as channel-to-channel and frame-to-frame comparisons.

However, before any target recognition algorithms can be applied, it is required to Fourier transform all the temporal signals from all the channels. As the size of the detector array and the channel data rates approach practical numbers, the possibility of using digital techniques for the Fourier transformation becomes more infeasible simply because of the volume of data. Other foreseeable problems with a digital approach include processor size and power consumption. To illustrate the potential scope of the signal processing problem, one can envision a 1000 x 1000 detector element array, i.e. 10^6 detector channels. Each channel could have 10^4 samples /sec data rate, and require a series of 128-point discrete Fourier transforms (DFT's) to be performed on the data train. Hence, on the order of 10^8 128-point DFT's per second are required. Since a 128-point DFT requires about 128 ($\log_2$ 128) = 896 complex multiplications, up to 10^{11} multiplications/sec are required. (State-of-the-art computers, such as ILLIAC IV and CRAY, are capable of 10^8 multiplies/sec.) The approach investigated here is the use of an acousto-optic Fourier transform device employing a chirp-Z algorithm in a time-integrating architecture. In the following sections the basic processor operation is described and the reasons are made clear why this particular processor is attractive for the Gemini application from the performance and package-size viewpoints. Also presented are experimental results obtained for both continuous and discrete Fourier Transforms, various concepts for implementations of compact processors, and some preliminary results for multichannel operation. The last section will describe future work and give recommendations for future developments required by the Gemini concept.

II. ACOUSTO-OPTIC FOURIER TRANSFORM DEVICE

Basic Processor Operation

There has been much recent work in the application of acousto-optics (A-O) to signal processing.[1] One of the main attractions of acousto-optics is that it affords a rapid, effective means of data input, with gigahertz bandwidth and good dynamic range acoustic devices now available. Combining the large bandwidth capability with the Fourier transforming properties of a lens allows for rapid processing of one-dimensional (1-D) signals. However, use of a lens to transform the information on an acoustic wave is not necessarily the best method of performing Fourier transforms in all instances. An alternative method for Fourier transformation is to employ chirp algorithms; this method possesses several advantages. For example, there is flexibility to optimize a desired parameter such as speed or resolution; data input can be in a variety of formats, and it is easier to obtain phase information compared to the lens-transform method. One particularly useful chirp algorithm is the following. The 1-D Fourier integral is defined as

$$F(\alpha\tau) = \int_{-\infty}^{\infty} S(t) \exp(-i\alpha\tau t)dt, \qquad (1)$$

where $\alpha\tau$ can be considered the frequency variable. Using the identity

$$-\tau t = 1/4\ [(t-\tau)^2 - (t+\tau)^2]$$

Equation (1) is changed into

$$F(\alpha\tau) = \int_{-\infty}^{\infty} S(t) \exp[+i(\alpha/4)\ (t-\tau)^2] \exp[-i(\alpha/4)(t+\tau)^2]\ dt. \qquad (2)$$

This algorithm is applicable for both continuous and discrete Fourier transforms and has been referred to as the triple-product-convolver algorithm[2], since there are now three input terms and the exponential terms in Eq. (2) are chirps of equal but opposite slopes. It is possible to implement Eq. (2) either with A-O[3] or with purely electronic filtering approaches.[4] However, use of the optical techniques to be discussed here offers additional advantages, as well as solutions to problems encountered with previous A-O approaches. For example, by using various time-integrating (TI) optical architectures, diode laser light sources, and the chirp algorithm represented by Eq. (2), one can obtain simplified and miniaturized processors, easy computation of either continuous or discrete Fourier transforms and increased data throughput. Both continuous and discrete Fourier transforms will be discussed below. Although either can be used, the use of the continuous transform appears to be more directly applicable to the Gemini situation.

Continuous Fourier Transforms

To implement Eq. (2), we have chosen to perform the multiplication by interference of information-carrying light beams (produced by acousto-optic diffraction) and to perform the integration by time-integration of the light signal on a detector array. The core of the optical signal processor is the modified Mach-Zehnder interferometer as shown in Fig. 3. An additive, time-integrating scheme was adopted rather than multiplicative ones such as described elsewhere.[5] The optical output of a diode laser, after collimation, is split into two beams of equal intensity by the first beamsplitter. Each beam is then directed through a Bragg cell. The laser diode beam was collimated along the direction transverse to laser junction

plane to maximize beamwidth, and compressed along the laser junction direction. The Bragg cells are so oriented that two positive first-order diffracted beams are produced. These diffracted beams are combined at a second beam splitter and detected by a square-law photodetector array. In this implementation of the Fourier transform, the Bragg cells are driven in the opposite directions by the same linear-FM (chirped) RF waveform. The Bragg-diffracted optical waves will be phase-modulated to yield the two exponential terms of opposite delays. The diode laser is intensity-modulated by the signal S(t). When the two diffracted fields are mixed in the square-law detector array and time-integrated over a period T, the electrical charge from the detector array consists of three terms: two bias terms proportional to intensities of the optical beams in the two legs of the interferometer, and a cross term containing the desired Fourier transform of the signal modulating the diode laser. Assuming that the path lengths and optical intensities in the two legs of the interferometer have been made equal, then the charge representing the cross term is:

$$q_T \propto 4\mathrm{Re}\ \{\exp(-2i\omega_0\tau) \int_0^T S(t)\ \exp(-2i\alpha\tau t)dt\}, \qquad (3)$$

if the linear FM RF wave is represented by $\cos\ [\omega_0 t+(\alpha/2)t^2]$, where ω_0 is the carrier angular frequency, α is the chirp acceleration, and τ is the time delay incurred in the Bragg cells ($=z/v$, where z is the spatial coordinate along the acoustic wave and v is the acoustic velocity in the Bragg cell). By recognizing $\alpha\tau$ as an instantaneous frequency, the integral in Eq. (3) becomes the Fourier transform of the signal S(t). Hence, the spectral information is impressed onto a spatial frequency $\omega_0/\pi v$. The frequency

resolution is approximately 1/T, the reciprocal of the detector integration time. The number of resolvable elements is $\alpha T \tau_{max}$, where τ_{max} is the maximum delay of the Bragg cell. The quantity αT is the chirp bandwidth. When an angle between the wavefronts of the two combined beams is introduced by changing the orientation of one of the turning mirrors, an additional phase factor $k_\ell \theta z$ should be included in the spatial carrier, where k_ℓ is the wave number of the optical wave and θ is the angle between the two wave fronts. This degree of freedom allows us to select the optimum value of the spatial frequency such that it is well resolved by the detector array.

Discrete Fourier Transforms

The discrete Fourier transform (DFT) is commnly used to transform sampled temporal data into the frequency domain, for applications involving discrete time or space variables, such as pulsed radar or array beamforming. The ability to optically implement the DFT involves proper formatting of the input data. For an A-O implementation, it is advantageous to implement the DFT as the discrete form of Eq. (2), i.e.,

$$F(k) = \sum_{n=0}^{N=1} S_n\,(t)\, \exp\left(\frac{i\pi(n-k)^2}{2N}\right) \exp\left(\frac{-i\pi(n+k)^2}{2N}\right) \qquad (4)$$

Here the required multiplications and summation are performed as described above for the continuous Fourier transform. A space-integrating (SI) scheme has been used elsewhere to obtain F(k).[6] In the SI scheme an N-point transform is obtained by using N light beams equally spaced along acoustic delay lines; each of the individual data points S_n is carried by a separate light beam as an intensity modulation; the multiplications are done via successive acousto-optic diffractions; and the light beams summed by focussing onto a

single photodetector. Here the data are inserted as a time sequence and the summation is achieved by time integration at the photodetector array. The SI scheme is appropriate if N parallel channels of data exist and it is not possible or desirable to time multiplex. The TI scheme is appropriate if the data are in a single temporal stream, either naturally or through multiplexing. A TI DFT processor has been investigated here because of its inherent simplicity of implementation and its potential for miniaturizat The data can be impressed onto the light beam via direct modulation of a de laser which offers compact size and high efficiency.

One can derive from Eq. (3) the manner in which the DFT is obtained with the TI processor and some of the characteristics of the transform output. If one considers a sampled data sequence of arbitrary values, one may express S(t) as

$$S(t) = S(nT_s) = \sum_{n=0}^{N-1} S_n(t)\, \delta(t-nT_s),$$

where T_s is the sampling period and $S_n(t)$ is the individual value of the nth data sample.

Thus the integral in Eq. (3) becomes:

$$\int_0^T S(t)\exp(-2i\alpha\tau t)dt \qquad (5)$$

$$= \sum_{n=0}^{N-1} S_n(nT_s)\, \exp(-2i\alpha\tau nT_s)$$

provided that $S_n(t) = 0$ for t outside of the integration interval (0,T). Equation (5) is, therefore, of the form of a DFT when the signal is a discrete data sequence. It can be expressed exactly in the form of a DFT, if $-2i\alpha\tau nT_S$ is made equal to $-2\pi ink/N$, i.e., $k = (\alpha zNT_S)/\pi v)$. The largest interval of k that can be observed is

$$\Delta k = \frac{2\alpha T z_{max}}{\pi v} \tag{6}$$

where z_{max} is the length of the illumination of the acoustic wave, and NT_S has been assumed to be equal to T. Thus, while it is obvious there is no limit on N (the input transform size), for large N the output display does not represent the entire transform space unless the remaining parameters on the right side of Eq. (6) are changed. However, it is very often advantageous to have a restricted output region, such as when a certain spectral region must be examined with high resolution. Output times or data rates are thereby reduced, since uninteresting regions of the spectrum are not covered.

From Eqs. (3) and (5) one notes that the detector output is

$$q_T \propto 4\mathrm{Re}\ [\exp(-2i\omega_0\tau) \cdot F(k)]\ ;$$

indicating that the envelope of the spatial carrier is the modulus of the DFT.

III. EXPERIMENTAL RESULTS

Discrete Fourier Transforms

To evaluate the performance of the TI DFT processor, experiments were carried out using equal-amplitude, equal-spaced pulses with the arrangement of Fig. 3. A 4-mW diode laser (single-mode under CW conditions) and bulk

$LiNbO_3$ Bragg cells (1-GHZ center frequency, 1% deflection efficiency/RF watt and 2- sec window) were used. Data was recorded from a 1024-element time-integrating Reticon array using a digitizing oscilloscope having 12-bit resolution. By reversing the phase of one of the chirps and substracting the result from the previous frame, one eliminated fixed pattern noise and signal-dependent bias terms. Each frame represented a 40 msec integration time. Transforms of data sequences consisting of different numbers of pulses were performed and the results are shown in Figs. 4 and 5. (The speckled appearance in the figures is due to the digitization of the spatial fringe carrier.) DFT's with N=4 and N=8 are shown in Figs. 4a and 4b, and those with N=64 and N=128, in Fig. 5. That Fourier spectra have been obtained is further supported by the results of simulation done on a waveform analyser (an FFT device). For comparison, the corresponding FFT spectra are also given in Fig. 4. The qualitative agreement is excellent, both following the expected $(\sin Nx)/(N \sin x)$ dependence. For transforms with large N, the window of the frequency output space given by Eq. (6) was not large enough to show any two adjacent principal lobes. Thus, in the case of the 128-point transform of Fig. 5, comparison was made of the peak-to-first-sidelobe ratio. This ratio is 0.23 as compared to a theoretical value of 0.212, again in good agreement. The symmetry of the sidelobes, however, does depend strongly on the chirp linearity and environmental phase perturbations such as vibrations and turbulence.

The maximum spectral component available in the output window is governed by the chirp bandwidth T and the maximum cell delay z_{max}/v, as indicated by Eq. (6). In practice, it is much easier to change T than to

change the latter, because of the limitations in Bragg cell sizes and materials.

It is possible to increase the speed and the throughput beyond what has been demonstrated, provided that the condition given by Eq. (6) is met. The present limit on the transform speed is the serial read-out time of the detector array (3 msec here). The read-out time, however, can be increased by use of faster clock circuits for the array (a factor of 10 is achievable with silicon-based devices such as the Reticon used here), or by use of special parallel readout arrays. The ultimate limit on the transforming time is the chirp duration. When large bandwidth, short duration chirps are used, there is a corresponding requirement for high-speed modulation of the diode laser over large dynamic ranges. Larger power output from the diode laser and higher Bragg cell deflection efficiency are also important considerations, since it is desirable to have the maximum output signal level at close to the saturation level of the detector array to fully use the dynamic range of the array.

Continuous Fourier Transforms

Continuous Fourier transforms were also demonstrated using the arrangement in Fig. 3. In this case the diode laser was operated CW at a half-maximum power level, and the information signal S(t) was added to the DC drive voltage. Single-frequency tones of up to 1 kHz were used for S(t). This frequency range is the one of most interest for Gemini applications and is obtained using chirp bandwidths of up to 10 MHz (See Eq. (6)).

The results obtained with a single tone at 200 Hz and with two simultaneous tones at 400 and 900 Hz are shown in Figs. 6 and 7

respectively. Peaks were produced at positions proportional to frequency, and the widths of the peaks obtained were inversely proportional to the integration time, as expected.

Dynamic Range

The devices used for initial experiments were not optimized for maximum dynamic range, since no attempt was made to optimize the Bragg cell deflection efficiency or the diode laser optical power. Optimum operation would require that the maximum output signal from the detector array be close to the saturation level so as to maximize the dynamic range utilization of the array for a given integration time (or frequency resolution). Some measurements, however, were carried out to determine the maximum dynamic range available under the earlier setup, and served to identify mechanisms that could limit dynamic range. Input dynamic range in initial experiments could only be maintained in the range of 20 dB for digital Fourier transformations with 40 msec integration time. Beyond this range, saturation occurred rapidly. The fact that a degradation in fringe visibility, relative to cw operation, occurred whenever the diode laser was operated in pulsed mode (biased at threshold) indicates that the coherence of the optical output has strong impact on the available dynamic range. Independent measurements on the spectral contents of the diode laser showed multimode emission under pulsed operations. Reported measurements of both the spatial and temporal coherence of pulsed diode lasers[7] support this view. We also observed that the reduction in visibility is not uniform across the output window. The observed phenomenon occurred to various degrees for different lasers, and suggests the strong need for single mode control under pulse modulation. A promising method for doing so using optical feedback injection locking has been reported.[8]

For the continuous Fourier transforms it is important to note that the dynamic range for the multiple-tone case is strongly affected by any non-linear response of the diode laser to the drive signal. Nonlinearities of the diode laser will lead to intermodulation-product signals.

Linear dynamic range can be increased by using for the diode laser an electronic drive circuit having feedback. The drive circuit maintains a linear relationship between the input signal level and either the drive current for the diode laser or the output light power (as measured by a photodetector which provides a feedback signal to the drive circuit). A circuit for linearizing the signal with respect to the drive current has been constructed and is shown in Fig. 8; this circuit has been applied to continuous Fourier transforms to ensure that the laser signal is not distorted with respect to the input signal, thereby introducing intermodulation signals. The results obtained using this circuit are shown in Fig. 9 and indicate a 30 dB dynamic range. The level for intermodulation products was measured by modulating the diode laser with a pure sinusoid and frequency analyzing the output of a photo-detector in the laser beam. Fig. 10a shows the purity of the sine-wave generator and Fig. 10b shows the laser-beam harmonic content when using the linearizing circuit of Fig. 8. Note that harmonics are all > 50 dB below the level of the fundamental response. The drive-signal level in this case corresponded to the 20 dB level of Fig. 9.

Compact Processors

Compaction of the Fourier transform architecture used here is desirable not only to achieve practical package sizes but also to minimize the lengths of non-common paths in this interferometric arrangement. The Mach-Zehnder

shown in Fig. 3 occupied a laboratory bench area of about 50 cm. by 25 cm. Compaction can obviously be obtained with shorter focal-length lenses and smaller optical components and mounts. Optical component miniaturization is finally limited by the size of the Bragg cells required to obtain desired frequency-band coverage. However, the TI architecture here offers further compaction capability because a variety of arrangements can be used to implement the basic algorithm (Eq. (2)). Several arrangements have been devised and demonstrated.

(1) One notes that an additive architecture was selected and implemented on a Mach-Zehnder interferometer as described earlier. However, the Mach-Zehnder can be folded back upon itself so that the original beam splitter also serves as the beam combiner for the two diffracted light beams. This scheme is illustrated in Fig. 11, and is essentially a Twyman-Green interferometer. This scheme has not been implemented, since it is a straightforward extension of the Mach-Zehnder.

(ii) The Twyman-Green arrangement still requires two separate Bragg cells, and the diffracted beams are not on a common path until the beam combiner is reached. By using bulk optic - surface acoustic wave (SAW) techniques developed recently[6] one can provide an entirely common path for the diffracted beams, while also having the two Bragg deflectors (SAW delay lines) on a common substrate. This scheme is illustrated in Fig. 12. Two SAW transducers are laid on opposite ends of a single substrate of $LiNbO_3$. Because of the anisotropic properties of Y-Z cut

cut $LiNbO_3$, by tilting the transducers relative to each other by the proper amount, two incident light beams can be made to interact independently, one with each SAW signal, without crosstalk between the two signals.[9] Therefore, one needs to generate the two incident light beams at the correct angles and in a compact system. Fig. 12 illustrates one way in which the two light beams were here generated. A bi-mirror was used along with a single light source. A common, folded path was used to simultaneously produce the angular separation of the two beams, the lateral beam expansion, and the vertical beam focussing. An alternative method that can be used to generate the two angled beams in a small volume is to use a beam-splitting prism such as used for laser doppler velocimeters.[10] However, the beam shaping optics then cannot occupy the same volume. On the exit side of the SAW line a single spherical lens re-collimates the light in the vertical direction and simultaneously acts as the first lens in a Schlieren system. Following a slit and the second Schlieren lens, the light is deflected vertically into the photodetector array for further compaction. DFT results have been obtained with this acousto-optic SAW processor. Results are identical to those described earlier, except for one further advantage. Because of the slower SAW velocity ($\sim 3.5 \times 10^5$ cm/sec versus $\sim 6.5 \times 10^5$ cm/sec for bulk $LiNbO_3$) and the low acoustic diffraction and attenuation (making longer acoustic lines possible) the observable interval of frequency space is larger (see Eq. (6)).

(iii) In the description of the basic TI processor above, it was noted that the same rf chirp waveform is used to drive both Bragg cells. The two differing waveforms required in Eq. (2) result from wave travel in opposite directions, since it is the spatial waveform that is of importance. By recognizing this spatial dependence it is possible to eliminate one of the Bragg cells and have two light beams impinge contra-directionally onto the remaining cell in a ring configuration.[11] This configuration is shown in Fig. 13. The paths for both light beams are exactly equal length and both encounter virtually identical perturbations. DFT results were obtained with this configuration. Stability against environmental perturbations was excellent. Phase reversals of one light beam can be used to eliminate fixed-pattern noise via frame-to-frame subtraction, as described earlier. These phase reversals were achieved here by inserting a microscope slide into one beam at a point where the two beams are separated. Phase reversal can also be perf med (inserting an electro-optic modulator into the ring and troducing a 90^{o} phase shift on each beam. This scheme has been the one pursued most actively in the recent experimental investigation.

Integrated optics must also be considered as a candidate approach for compact devices. The TI bulk optics -SAW processor above could be implemented on a structure very similar to the integrated-optic rf spectrum analyzer demonstrated recently.[12] A method for producing two coherent, angled light beams within the waveguide layer is needed, and a method for rejecting undiffracted light (e.g., polarization rejection) may need to be perfected if

a Schlieren system is impractical due to substrate size requirements. One possible disadvantage of integrated optics is that it is limited to planar geometries. Integrated optics may in fact be best suited to the SI DFT architecture.(6)

Multichannel Processing

The number of Fourier transforms required in the Gemini concept probably dictates a scheme where many Fourier transforms are performed in parallel. If data is handled in real time, the time required to perform the Fourier transform is inversely proportional to the frequency resolution required and is therefore fixed. The alternative is to digitally store all of the data and then use time-base compression for insertion into a fast processor the multiplexed data. If all the data from an entire array is handled digitally, the A/D requirements are very large and the times for insertion and retrieval from memory could be the limit rather than the transform time. Some limited amount of multiplexing, however, should be feasible, but this would still imply multichannel operation.

The characteristics of the time-integrating Fourier-transform processor described above lend itself easily to multichannel operation for large throughput. Since the chirp waveforms are independent of the signal (although synchronized with it) multichannel operation does not require any replication of the acoustic cells. A multiplicity of input channels can be obtained using any of a variety of techniques. Fig. 14 illustrates one technique using an array of laser diodes and a corresponding array of lenslets. Detection is then done with a two-dimensional time-integrating photodetector array, each row of the array corresponding to a different processing channel.

Alternatively, it is possible to use a parallel-addressed one-dimensional spatial light modulator to provide multi-channel modulation of a single, wide laser beam. Candidate modulators include total internal reflection electro-optic devices that require only 5V for full contrast and which can be addressed using microelectronic structures.[13] Use of microelectronic structures has been shown to provide a potential capability of more than 5000 independent channels on a single crystal-microchip assembly.

To demonstrate the concept, we have set up a two-channel experiment as shown in Fig. 15, using the single-cell ring configuration. The beam from channel two is set slightly above the beam from channel one. The outputs of the channels are projected directly onto a 100x100 Reticon detector array, and the fringe patterns are displayed on an x-y-z CRT scope. A typical case is shown in Fig. 16. Figure 16(a) shows the fringe patterns obtained with different CW signals on the two channels (channel 2 is above channel 1). Figure 16(b) shows the two autocorrelation peaks of both channels when a 40 msec RF chirped pulse is applied to the Bragg cell. Note the fringe pattern under the peaks and the bias level elsewhere. Fig. 16(c) shows the difference in the two channels when the diode laser source of channel 2 is modulated by a 120 Hz sinewave. The positive part of the sinewave spectrum is shown to the right of the DC peak in the upper trace.

A one-dimensional spatial light modulator scheme is also being investigated. A design has been completed and fabrication initiated on an 8-channel array of modulators. Each modulator is of the design shown in Fig. 17, consisting of interdigital metal electrode fingers on an electro-optic substrate such as $LiTaO_3$. Electrical signals applied to the electrodes result

in index-of-refraction changes in the substrate, which in turn changes the phase of a light beam totally internally reflected off the substrate face. Finally, a phase-contrast readout system converts the phase changes into intensity modulation. The designed 8-channel device will have the following characteristics:

(1) 8 channels, with the interdigital finger patter of each channel covering 15 mm by 2 mm.

(2) Maximum drive voltage of 5 volts

(3) Frequency range of modulation, DC - 300 kHz

(4) Rise time of modulation < 25 nsec.

IV. SUMMARY AND RECOMMENDATIONS FOR FUTURE WORK

This effort has resulted in a number of significant accomplishments towards the development of a practical acousto-optic Fourier-transform device to address the signal-processing problems for Gemini. A time-integrating chirp-Z acousto-optic architecture has been identified as the basic building block. For this processor, the following have been shown.

- Both discrete and continuous Fourier transforms can be calculated.
- Continuous transforms can be applied in the frequency range of interest for Gemini.
- Concepts for inherently compact processors have been proven. In particular, a 1-cell ring configuration shows promise.
- Dynamic range of 30 dB has been demonstrated for a single CW signal and of > 20 dB for multiple signals. Increased dynamic range has been achieved using feedback drive circuits for the diode lasers.

o Feasibility of multichannel processing for simultaneous computation of several Fourier transforms has been demonstrated.

Multichannel operation using an 8-channel modulator is planned. The 8-channel modulator will be delivered in October 1982 by Xerox Electro-Optic Systems.

Beyond the above accomplishments, additional developments/demonstrations that will be required can be identified and include:

(i) Use of optical feedback from the laser beam to increase the linear dynamic range.

(ii) Investigation of diode lasers with higher powers and better linearity.

(iii) Testing of the processor with simulated, but realistic, Gemini signals.

(iv) Expanded multichannel operation beyond eight channels. A significant effort will be needed to obtain a processor of the size and robustness required by applications foreseen for Gemini. Concepts for obtaining the inherent size capability have been investigated here. Engineering of the miniaturized optical systems for such a processor can advantageously draw upon recent work to develop a miniature rf acousto-optic Bragg cell spectrum analyzer (package size < 10 in^3).

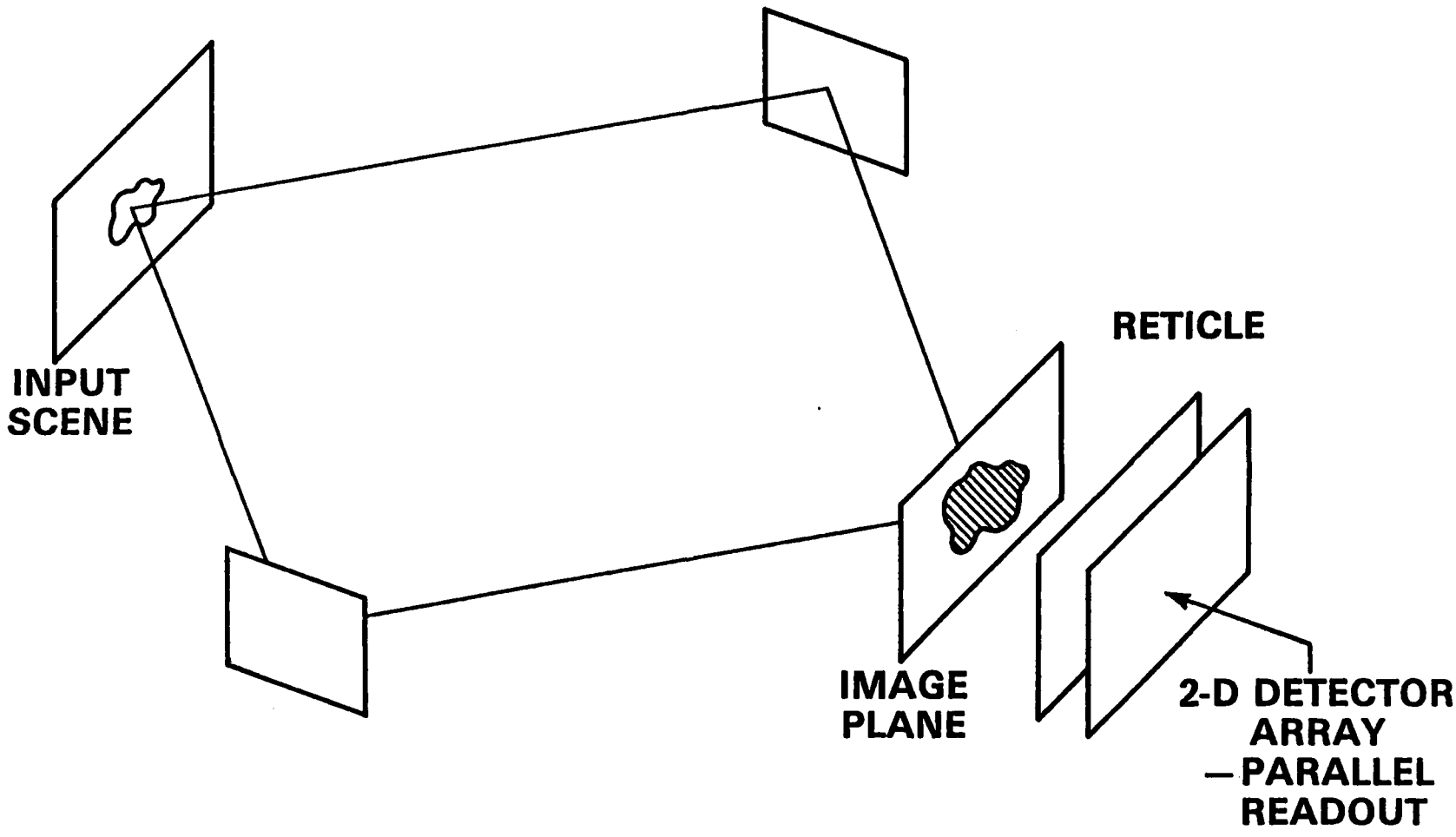

Fig. 1. Schematic of the Gemini concept.

Optical Transfer Function Defines Electrical Spectrum

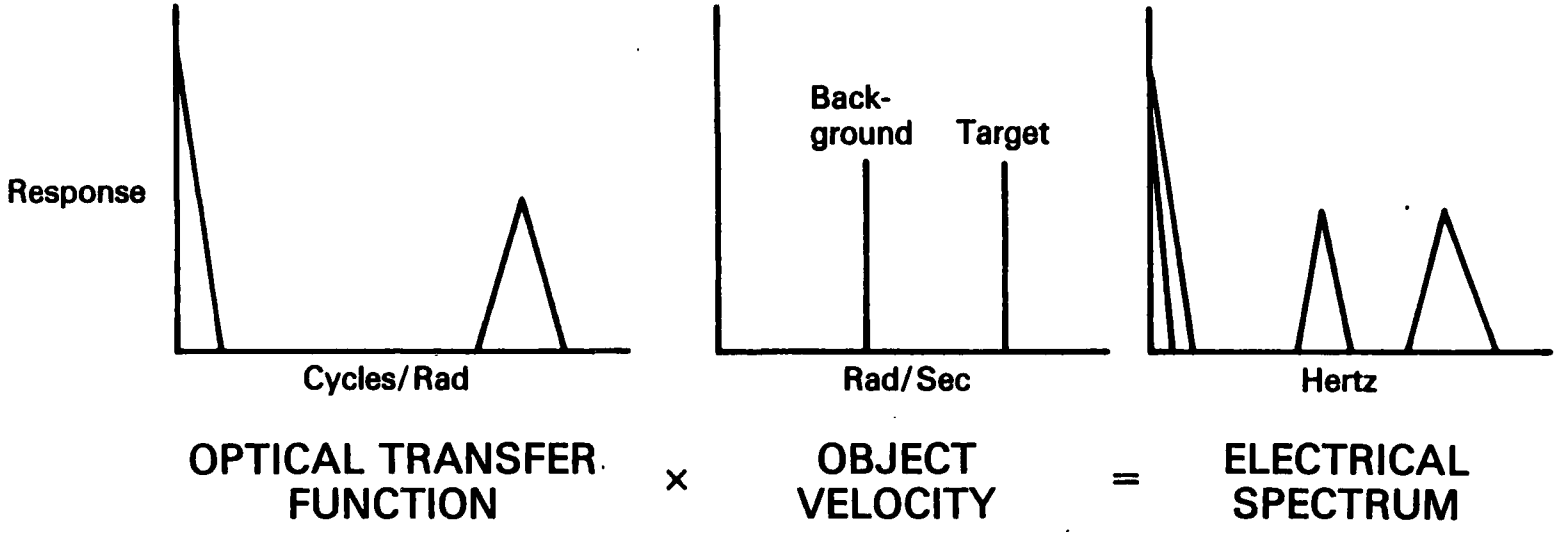

Fig. 2. Electrical Signal Spectrum as generated by the optical transfer function of the optical system.

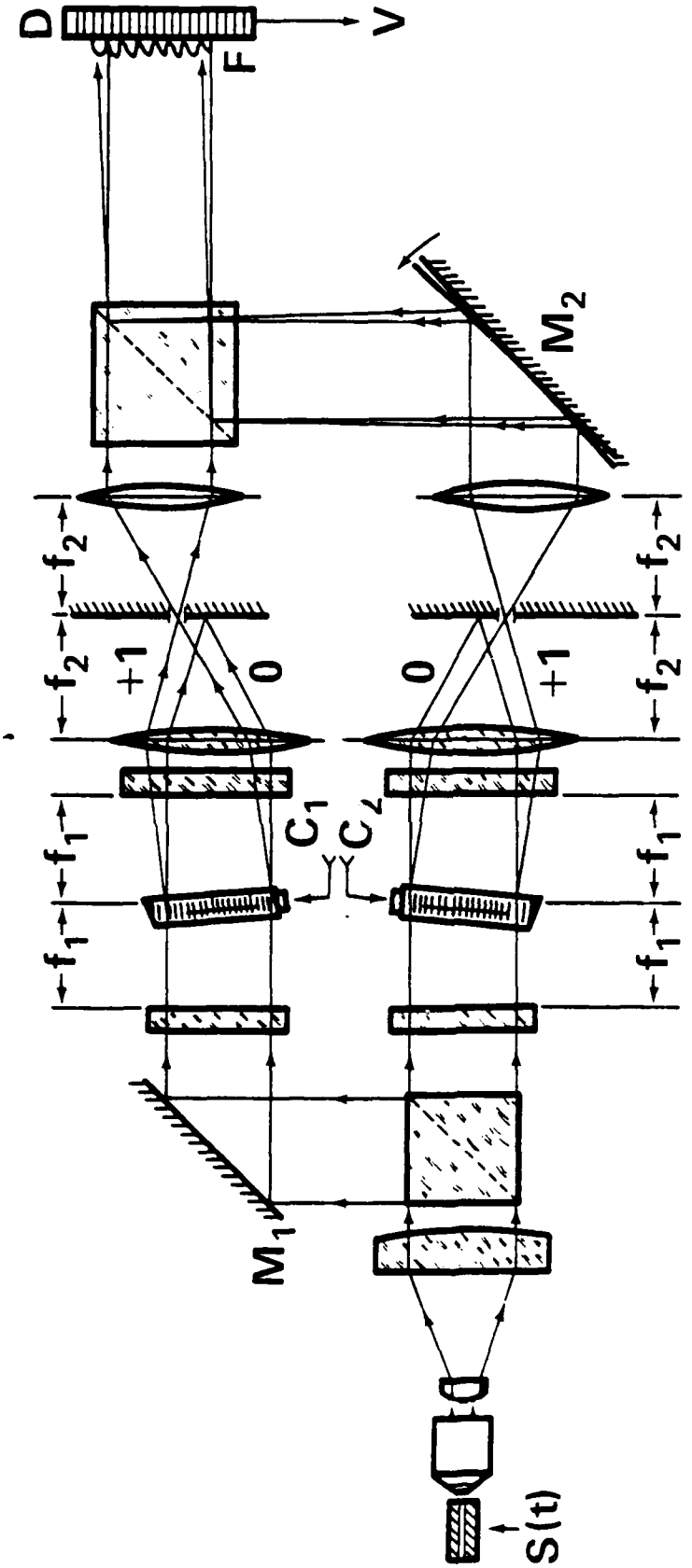

Fig. 3. Experimental arrangement for time-integrating, acousto-optic DFT processor.

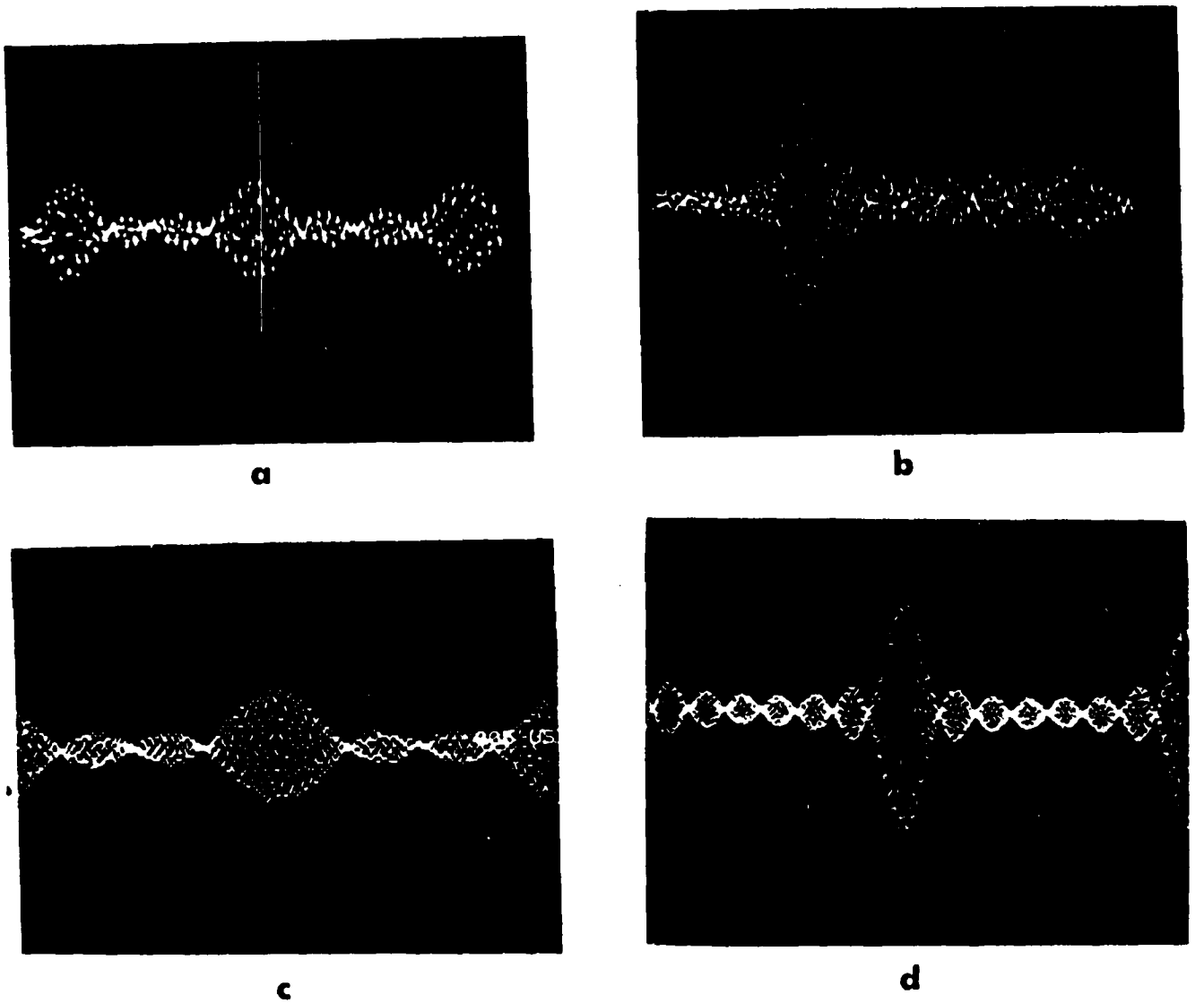

Fig. 4. Results obtained with the DFT processor on an equi-spaced, uniform amplitude pulse train consisting of (a) 4 pulses and (b) 8 pulses with the corresponding FFT results (c) and (d), respectively.

Fig. 5. Result obtained with the DFT processor on an equi-spaced, uniform amplitude pulse train consisting of 64 (left) and 128 (right) pulses.

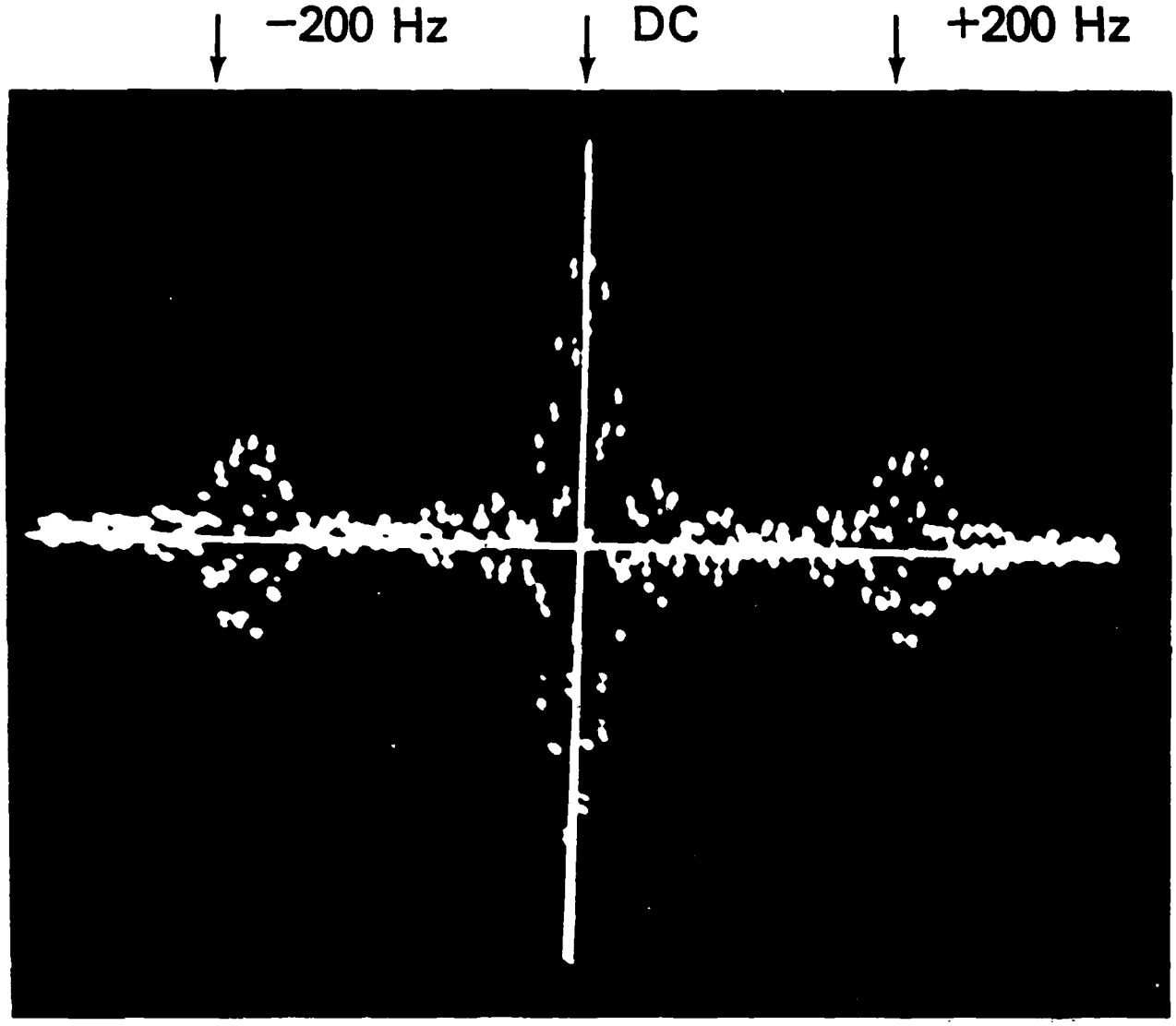

Fig. 6. Spectrum of a biased sinusoidal wave signal of 200 H_z.

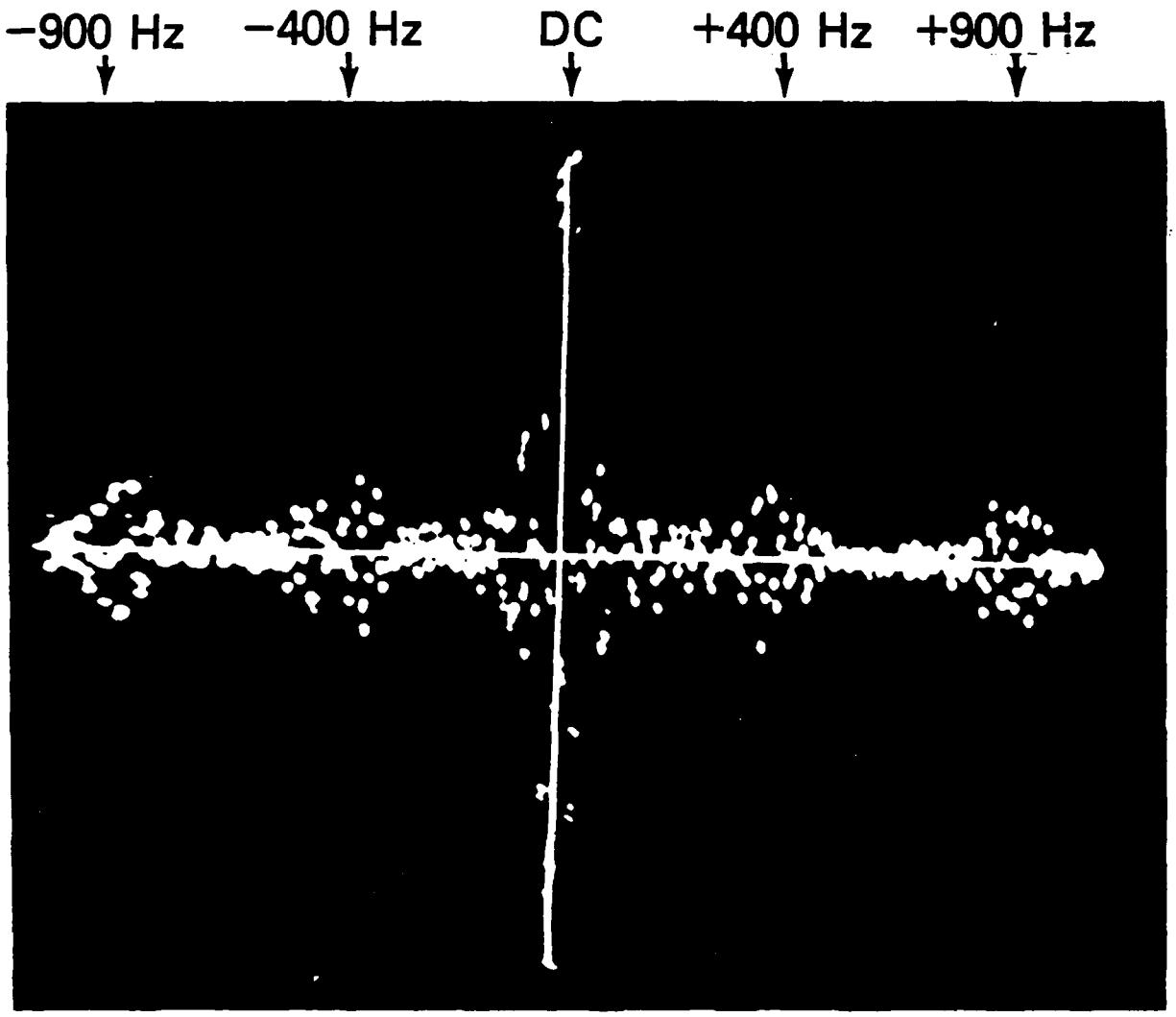

Fig. 7. Spectrum of a dual sinusoidal signal of frequencies 400 H_z and 900 H_z.

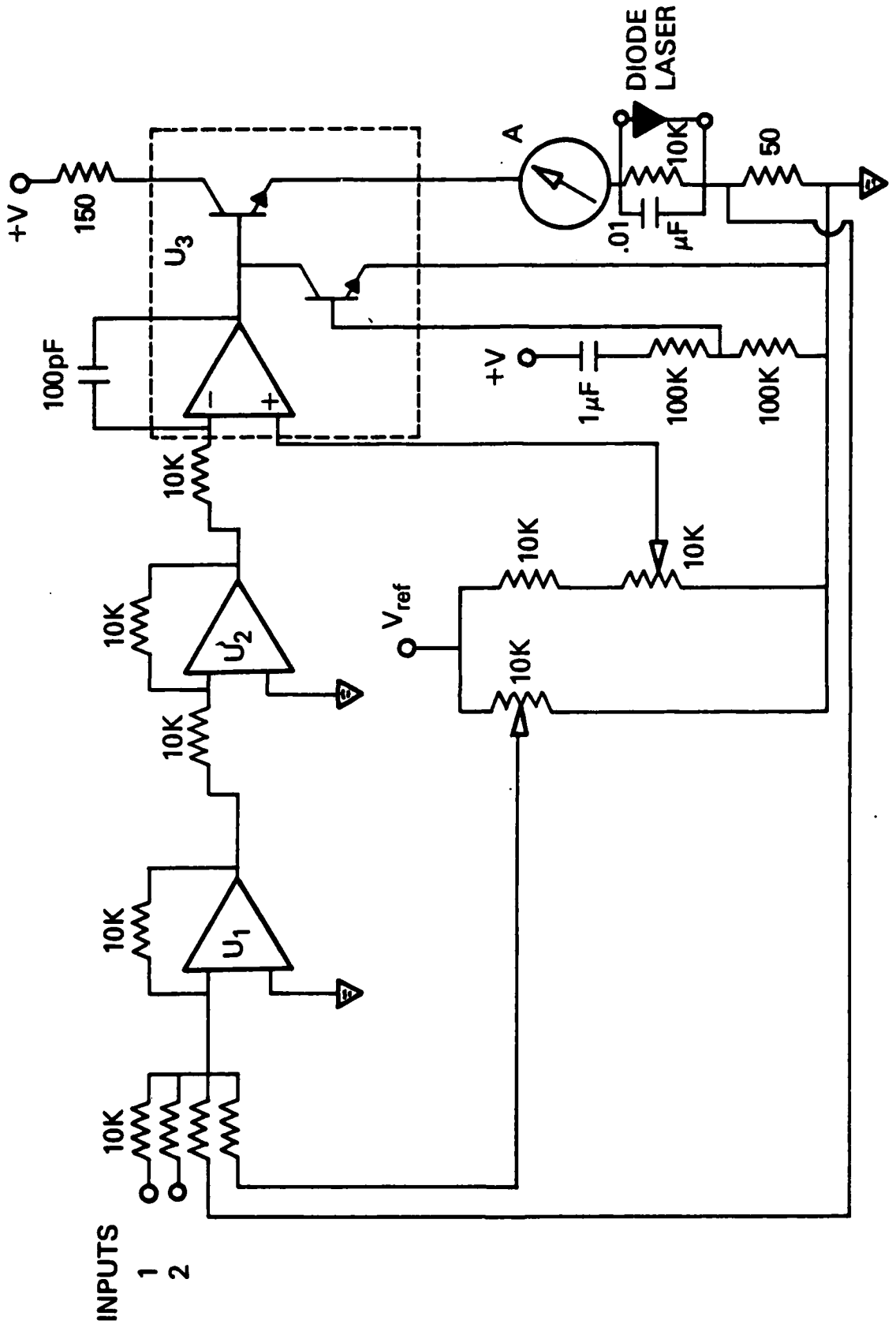

Fig. 8. Electronic circuit diagram for the diode laser current modulator.

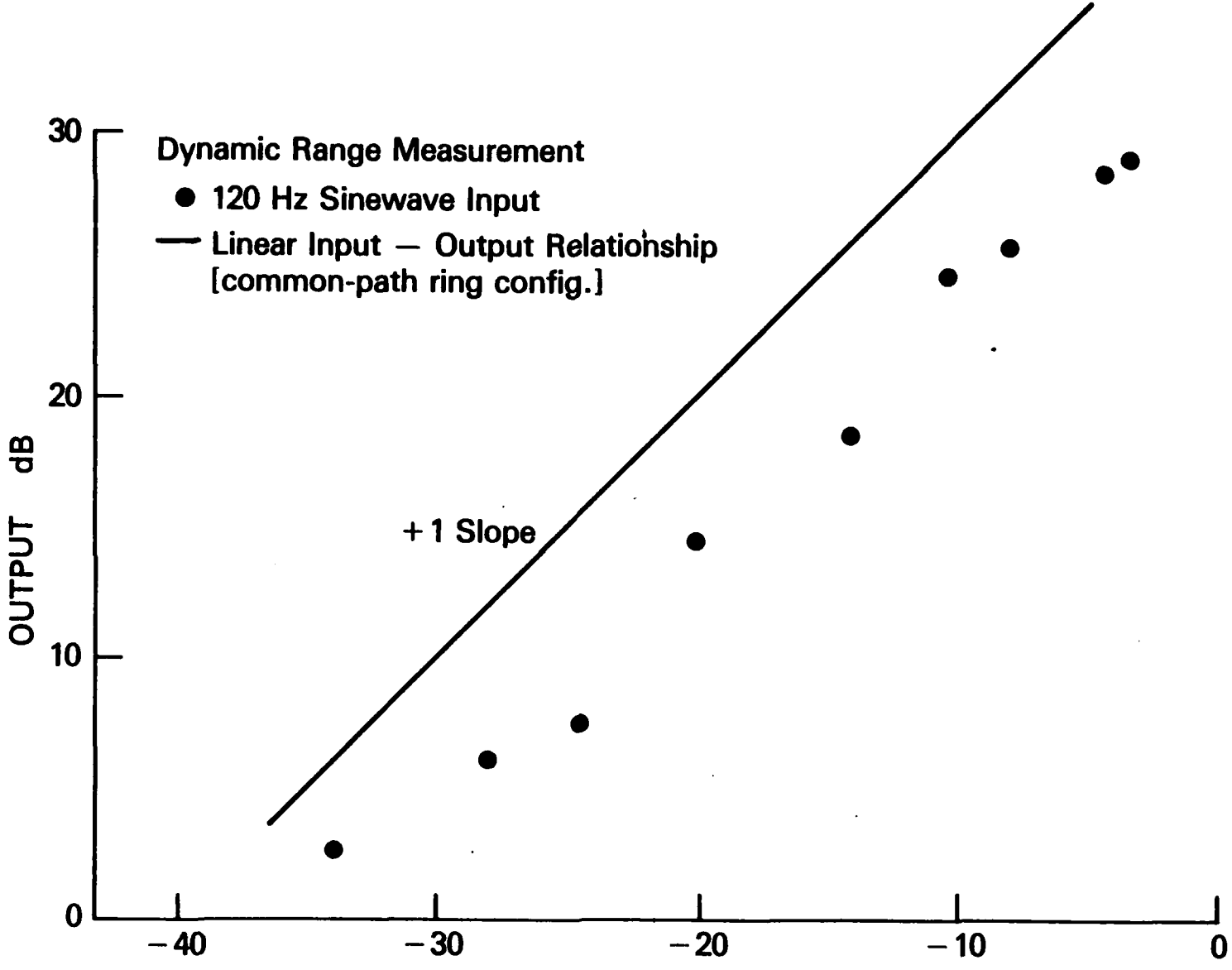

Fig. 9. Measured dynamic range of the processor.

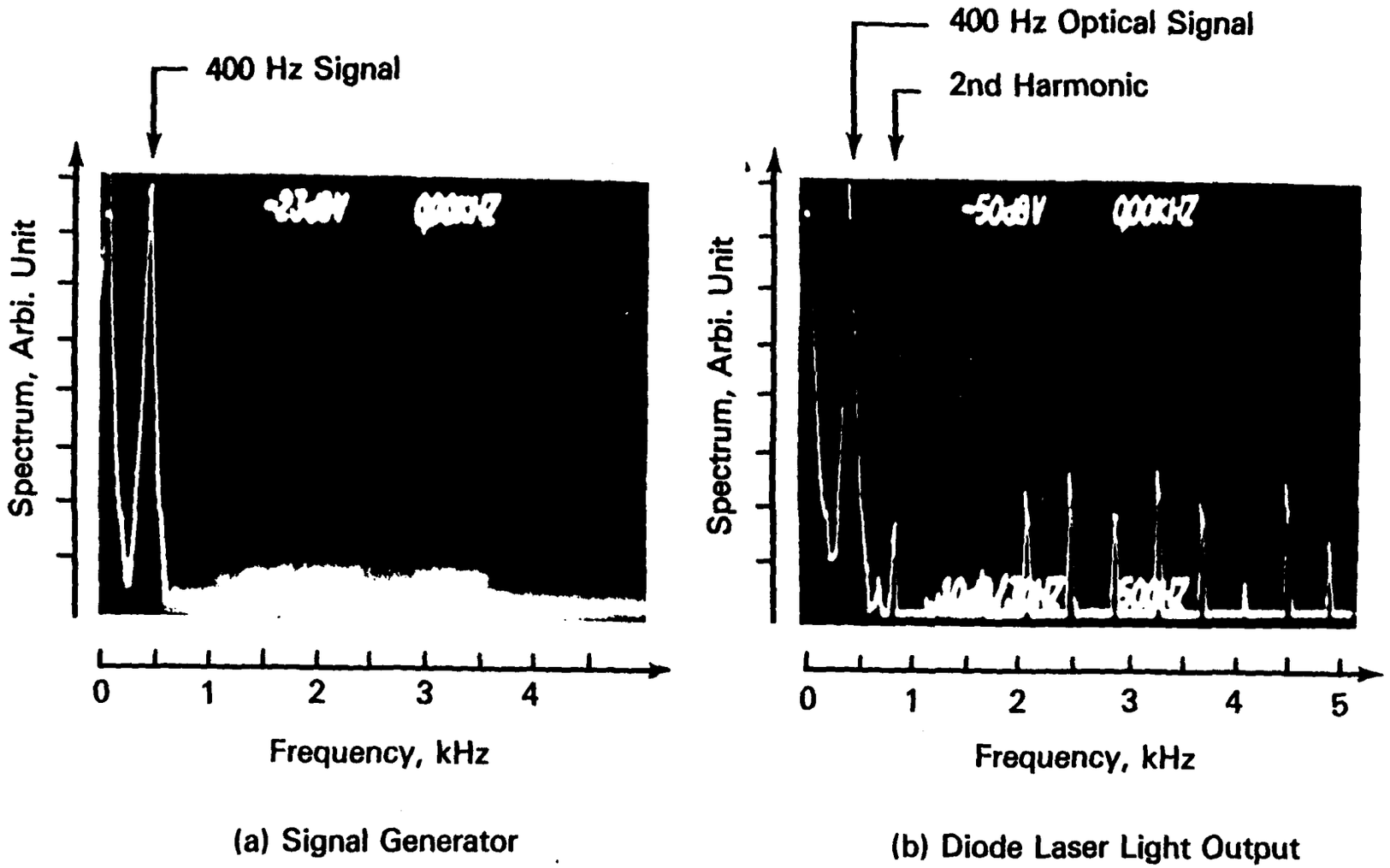

Fig. 10. (a) Spectrum of the signal generator of pure tone of 400 H_z, and (b) the spectrum of the diode laser light output when modulated by the 400 H_z signal. The second harmonics and the higher orders are 50 dB below the fundamental.

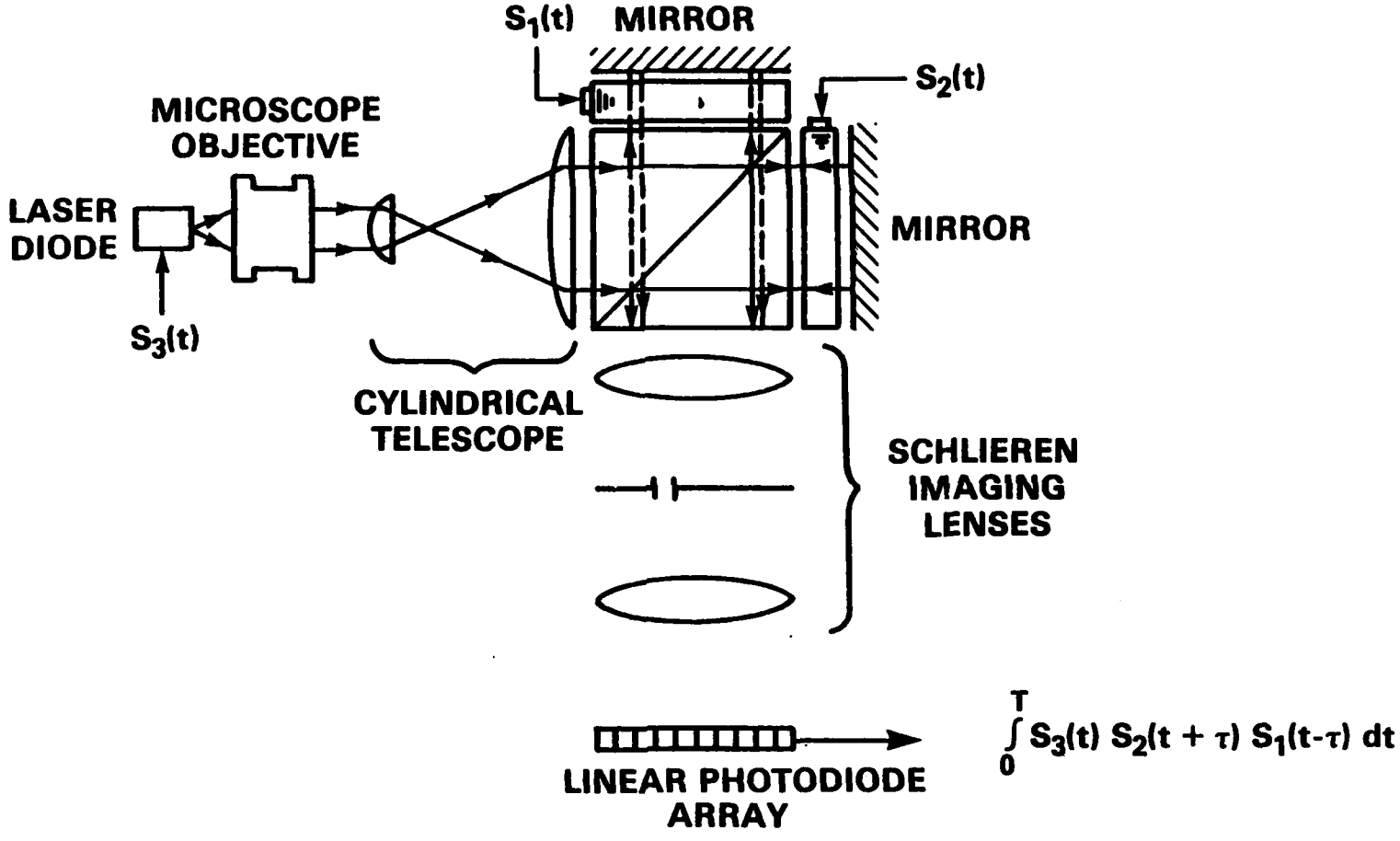

Fig. 11. Fourier transform processor using Twyman-Green arrangement.

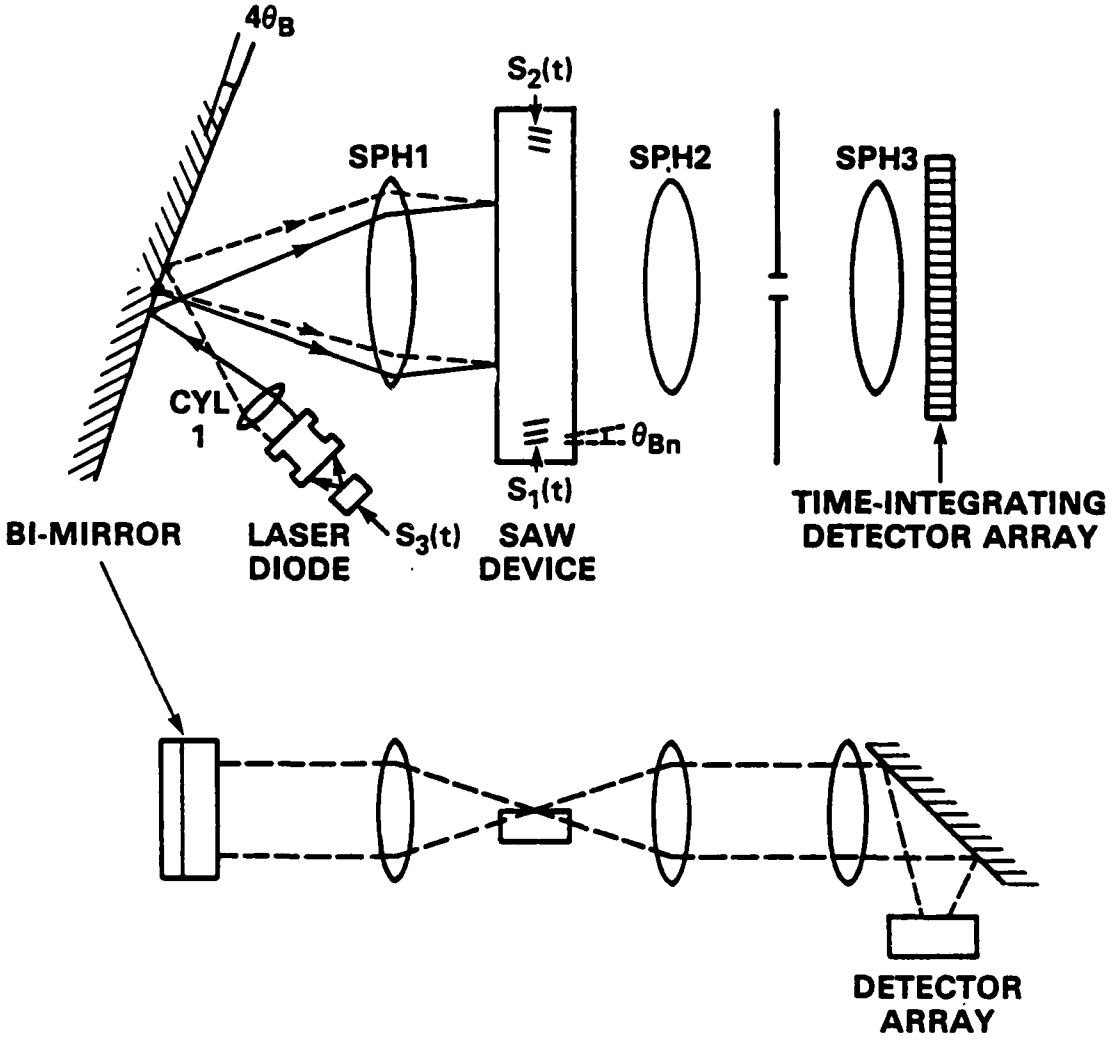

Fig. 12. Bulk optics and SAW Fourier transform processor.

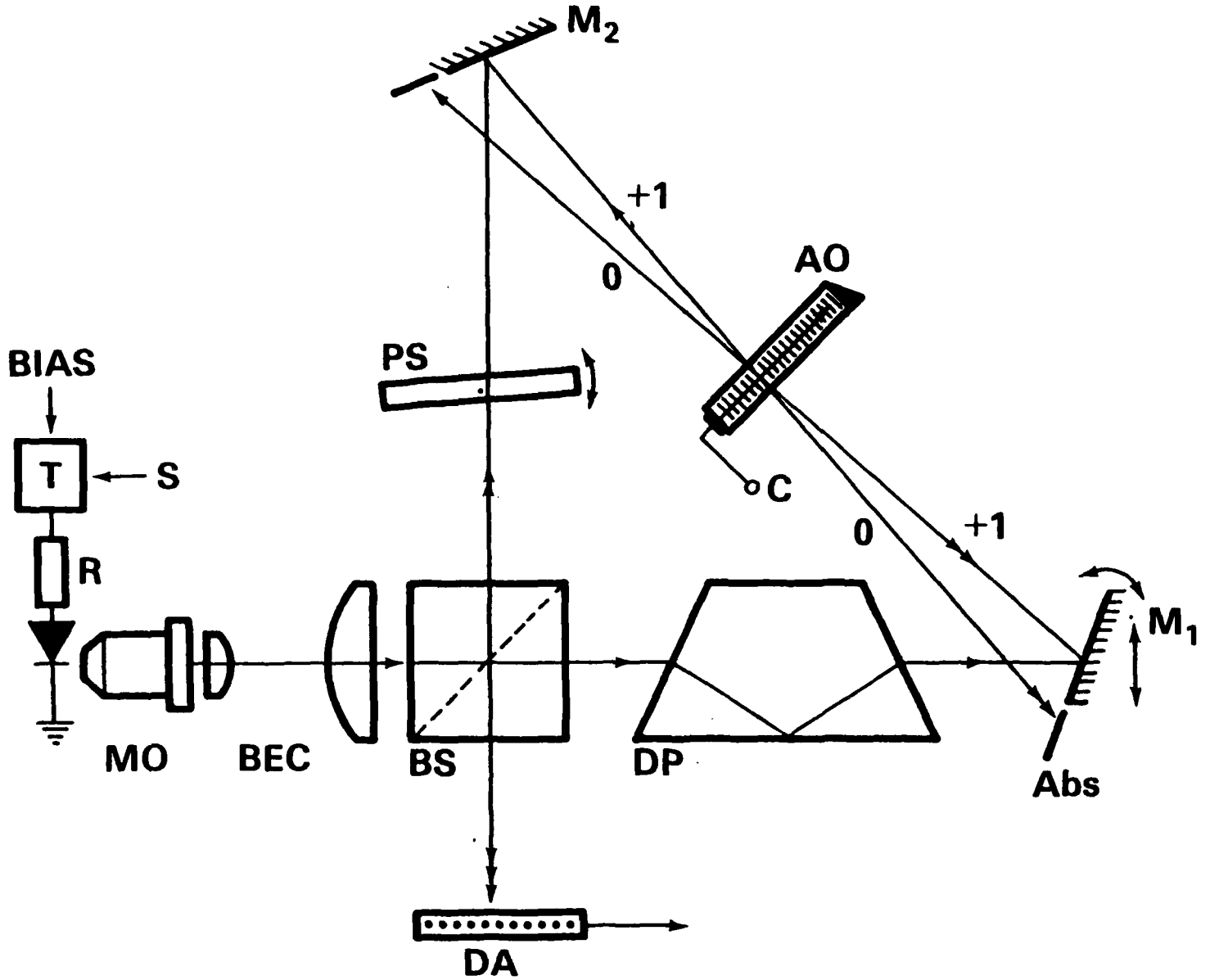

Fig. 13. Fourier transform processor using only one Bragg cell in a ring interferometric configuration.

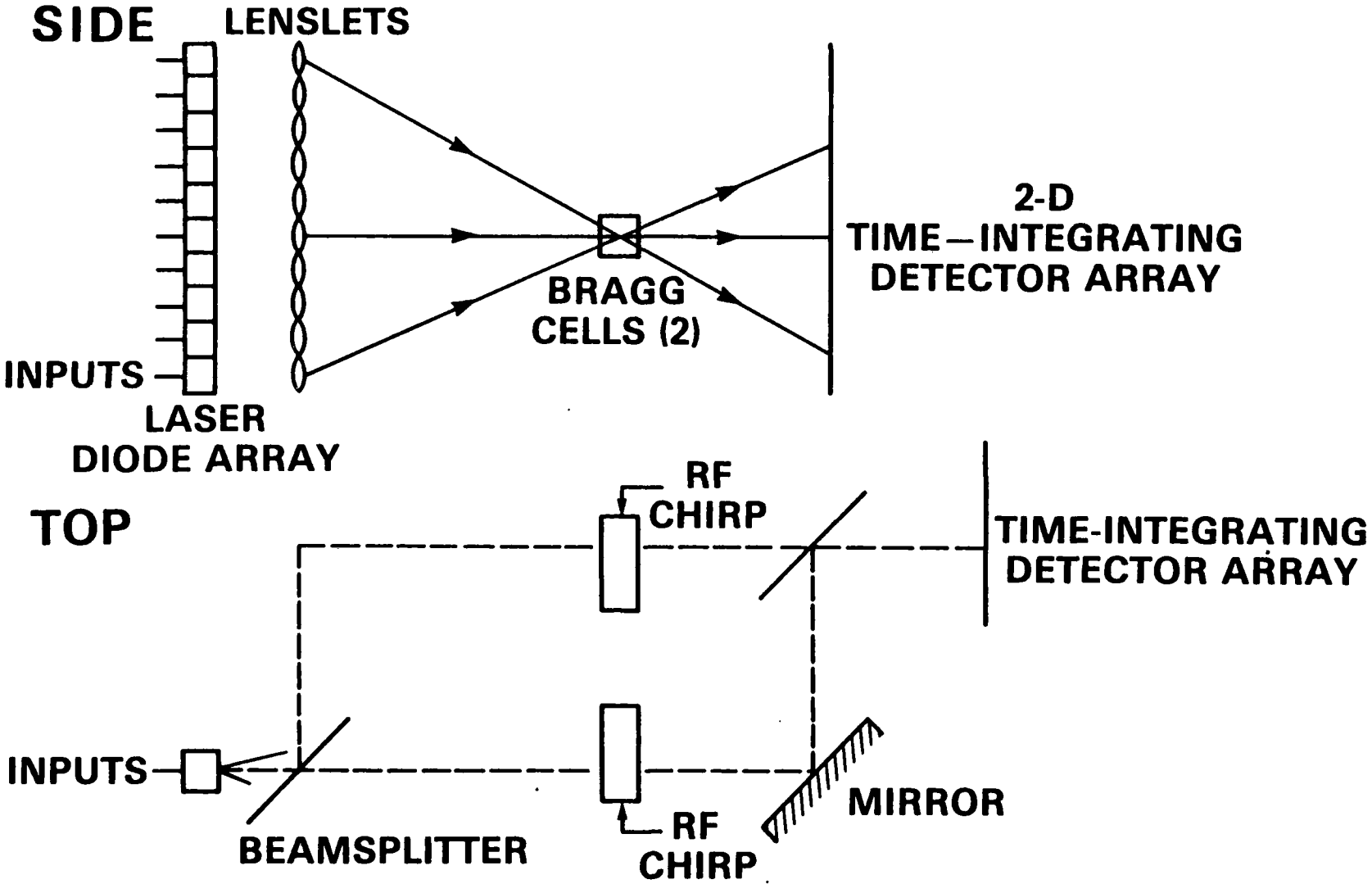

Fig. 14. Multichannel concept of the signal processor using diode laser array.

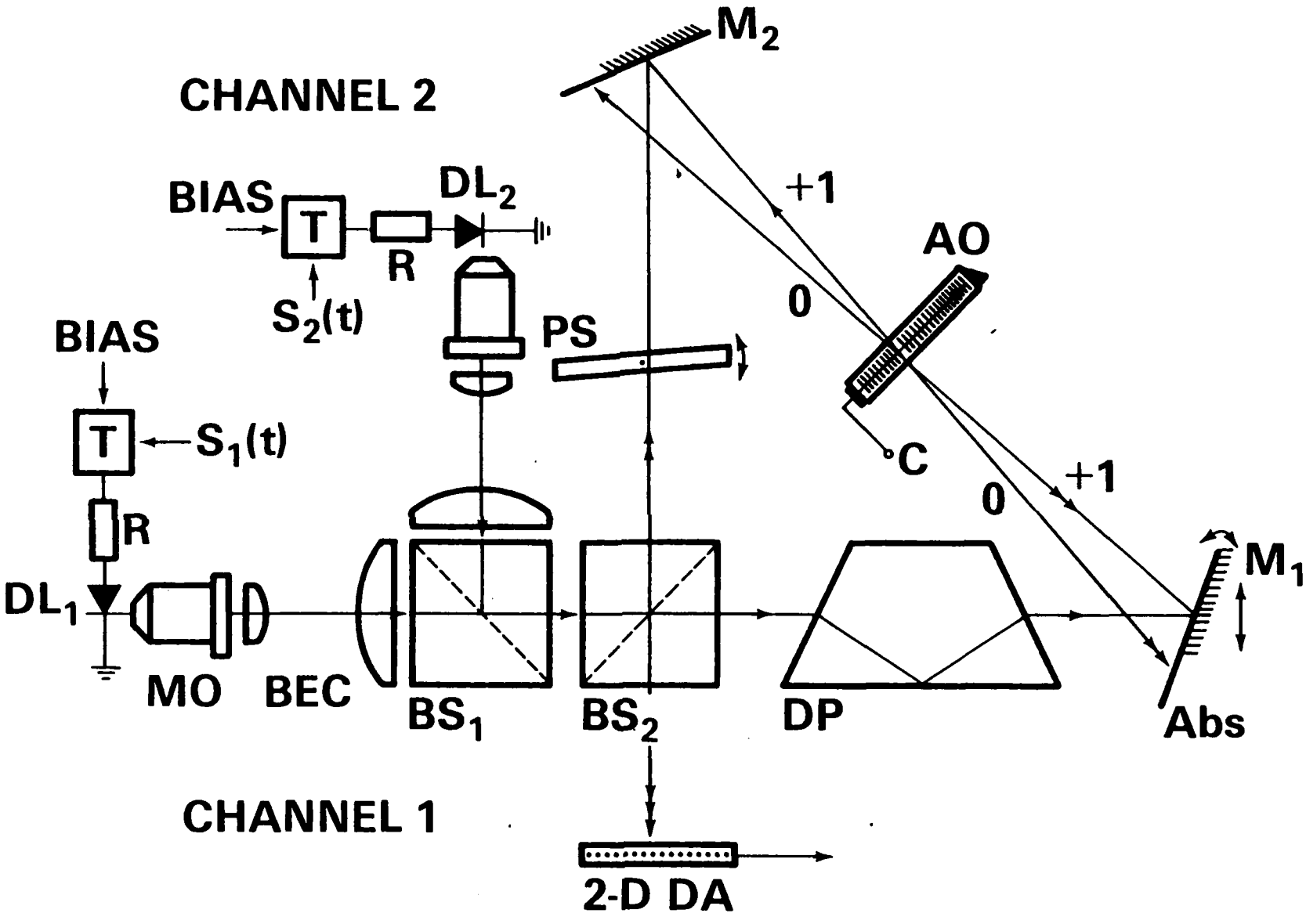

Fig. 15. Two-channel TI FT processor based on the ring interferometric configuration - experimental setup.

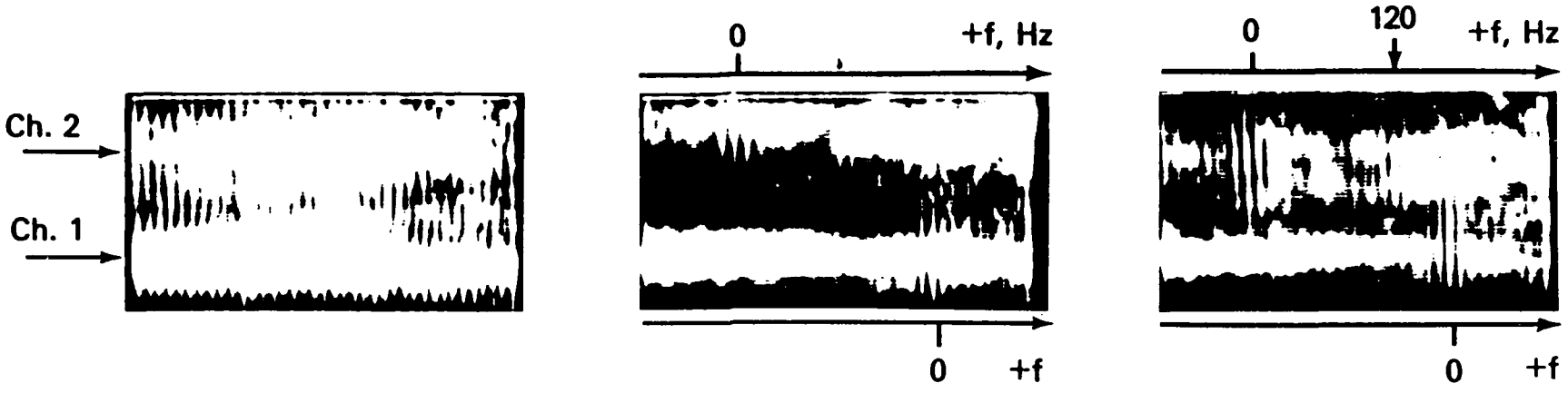

(a)
CW Fringes

(b)
Chirp Autocorrelation
in both channels

(c)
Fourier transform
of 120 Hz sinewave
in Channel 2.

Fig. 16. Results of the two-channel processor as recorded by a 100x100 detector array.

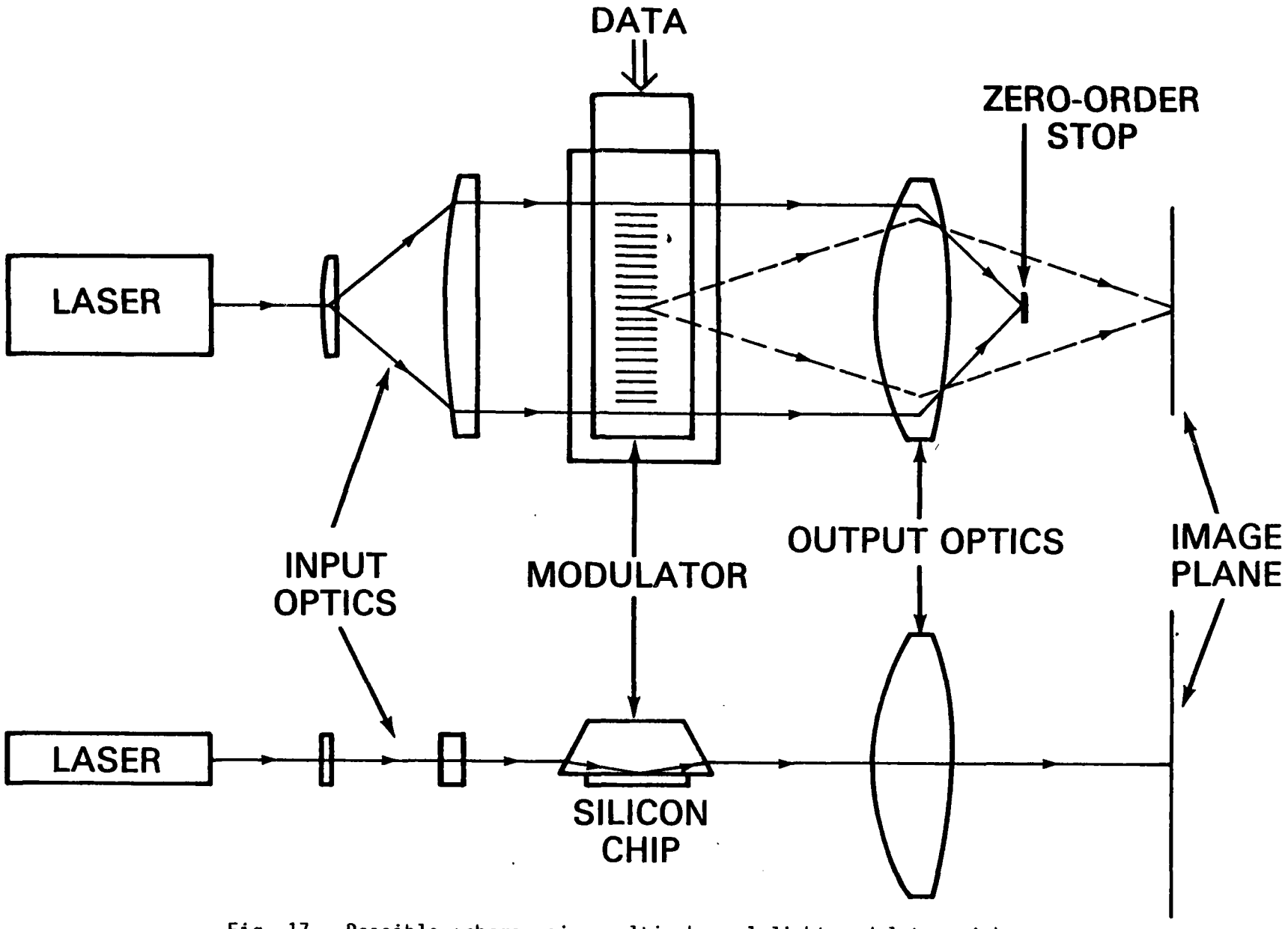

Fig. 17. Possible scheme using multi-channel light modulator with one laser source for multichannel processor implementation.

References

1. For recent review see articles in the January issue of the Proc. IEEE, 69, (1981).
2. J. M. Speiser and H. J. Whitehouse, NUCTN 1355R, Naval Ocean Systems Center, San Diego, California (1974).
3. W. D. Squire, H. J. Whitehouse and J. M. Alsup, Proc. Electro-Optics Conf., England 153 (1971).
4. R. C. Williamson, Proc. Soc. Photo-Opt. Instr. Eng. 185, 74 (1979).
5. T. M. Turpin, Proc. IEEE 69, 79 (1981).
6. N. J. Berg, J. N. Lee, M. W. Casseday, and B. J. Udelson, Applied Optics 18, 2767 (1979).
7. S. P. Kalashnikov, I. I. Klimov, V. V. Nikitin, and G. I. Semenov, Sov. J. Quantum Electron, 7, 946 (1977).
8. K. R. Preston, K. C. Wollard, and K. H. Cameron, Electronics Letters, 17, 931 (1981).
9. J. N. Lee, N. J. Berg and M. W. Casseday, IEEE J. Quantum Elec, QE-15, 1210 (1979).
10. See for example models by Malvern Scientific, Inc.
11. S.C. Lin and A. B. Tveten, "A Simplified Time-Integrating Acousto-Optical Processor for Fourier Transformation," to be published in Optics Letters, September 1981.
12. D. Megerian, E. C. Malarkey, R. P. Pautienus, J. C. Bradley, G. E. Marx, L. D. Hutcheson and A. L. Kellner, Applied Optics, 19, 3033 (1980).
13. R. A. Sprague, W. D. Turner, and L. N. Flores, Proc. Soc. Photo-Opt. Instr. Eng. 299, 68 (1982).

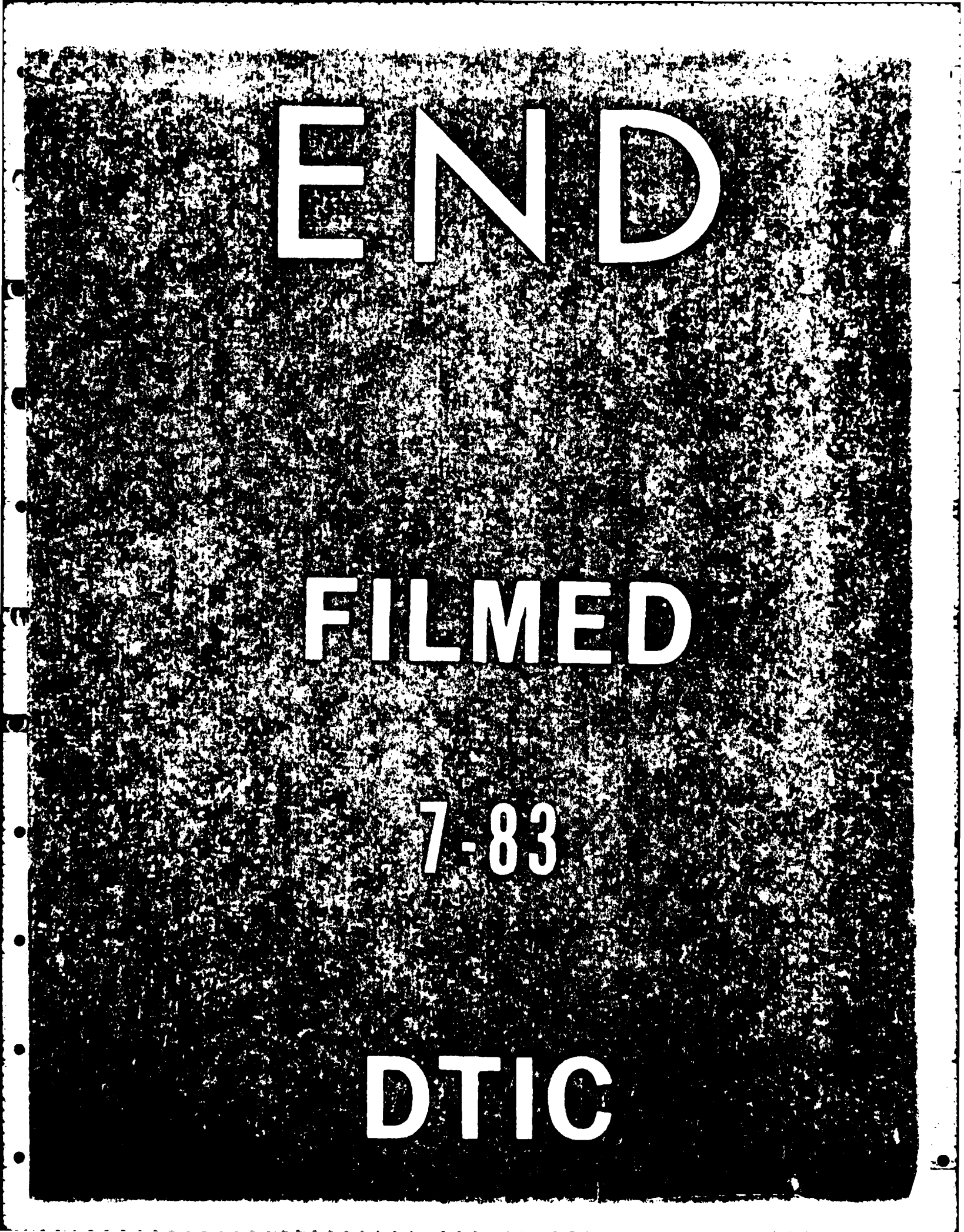
END
FILMED
7-83
DTIC